DOI: 10.3969/j. issn. 1673-5188. 2017. 01. 003
http://www.cnki.net/kcms/detail/34.1294.TN.20170220.1110.002.html, published online February 20, 2017

A Survey of Massive MIMO Channel Measurements and Models

ZHANG Jianhua, WANG Chao, WU Zhongyuan, and ZHANG Weite
(Beijing University of Posts and Telecommunications, Beijing 100876, China)

Abstract

Compared with conventional multiple-input multiple-output (MIMO), massive MIMO system with tens or even hundreds of antennas is able to give better performance in capacity and spectral efficiency, which is a promising technology for 5G. Considering this, massive MIMO has become a hot research topic all over the world. In this paper, the channel measurements and models of massive MIMO in recent years are summarized. Besides, the related 256 antenna elements with 200 MHz bandwidth at 3.5 GHz proposed by our team, the verification of rationality of the measurement method, and the spatial evolution of clusters in mobile scenario are provided.

Keywords

massive MIMO; channel measurement; channel model; virtual measurement; cluster

1 Introduction

Mobile traffic is predicted to grow more than 1000 times in the next 10 years, and the International Mobile Telecommunication (IMT) vision towards 2020 and beyond requires future 5G systems to deliver a 10 Gbps peak data rate. Considering this, more and more work is turning to the massive multiple-input multiple-output (MIMO) technology. Compared to the current state of the art, massive MIMO system has a large number of antennas, typically tens or hundreds, and provides better performance in efficiency, capacity, reliability and more [1]–[3]. It can improve channel capacity, can reduce latency on the air interface, and is robust against unintended man-made interference and intentional jamming [4], [5]. However, it brings increasing complexity of channel modeling.

Therefore, a series of massive MIMO measurement campaigns have been performed to evaluate the channel performance. For example, outdoor channel measurements at 2.6 GHz with a linear virtual array and a cylindrical array of 128-element antennas are reported in [6] that studied the sum-rate capacity, spectrum efficiency, precoding schemes, etc. In [7], an outdoor static measurement performed in a stadium is analyzed, with a linear 128-element antenna virtual array at 1.4725 GHz and the angular power spectrum (APS) in the massive MIMO channel. The modeling of massive MIMO channel has also been studied. Moreover, spatial non-stationary properties should be considered in the model in response to the larger antenna array and near field effect. In this paper, massive MIMO channel measurements and modeling in recent years are reviewed. Section 2 discusses the recent measurement campaigns. The modeling work of massive MIMO is given in Section 3. Section 4 displays the work of our team, which analyzes the rationality of virtual measurement and the spatial evolution of clusters in the mobile scenario of massive MIMO. Finally, the conclusions are drawn in Section 5.

This research is supported in part by National Natural Science Foundation of China (61322110, 6141101115), in part by National Science and Technology Major Project of the Ministry of Science and Technology (2015ZX03002008), in part by National Key Technology Research and Development Program (2012BAF14B01), by "863" Program (2015AA01A703), and by Doctoral Fund of Ministry of Education (20130005110013).

2 Massive MIMO Channel Measurements

Channel measurements are indispensable in research of wireless communications. Here a series of massive MIMO measurement campaigns in recent two years are listed. **Table 1** gives thesetups and investigated channel characteristics of these measurements.

2.1 Capacity

With the increase of the antenna number, massive MIMO systems can improve spectral efficiency significantly. In [8], 128Tx-16Rx massive MIMO is found to provide up to 434%

Table 1. Summary of massive MIMO channel measurements proposed in recent two years

Antenna array setup	Scenario	Carrier frequency (GHz)	Channel characteristics	Reference
Tx UPA/Rx ODA 16×16	UMi	3.5 and 2.35	Capacity; eigenvalues	[8]
Tx UPA/Rx ODA 32×56	UMa, O2I	6	Angle spread; delay spread; channel capacity	[40]
Tx UPA/Rx ODA 32×56	O2I	6	Delay spread; angular spread; capacity in different height	[41]
Tx UPA/Rx ODA 32×56	UMa	3.5	The rationality of virtual massive MIMO measurement	[34]
Tx UPA/Rx ODA 32×56	UMa mobility	3.5	Cluster number; cluster-AoA; cluster-AoD; radius of visibility region	[35]
Rx/cylindrical 24×2	O2I, UMi, UMa	2	Capability	[9]
Tx/cylindrical 32×4	indoor	19.85	SNR	[15]
Virtual linear 12×12	lecture hall	5.6	Condition number; delay spread variation	[11]
Tx/virtual circular 24	vehicle to infrastructure	2.6	SIR; power density	[42]
Rx/horn antenna 1	O2I	2.59	Correlation coefficient; SNR	[12]
Rx/2D virtual 12×12	UMa	2.53	Angle delay; angle spread.	[22]
UPA 4×4	indoor	2.4	SNR	[10]
Horizontal 64×1/ vertical 1×64	UMa, UMi	2.6	SNR	[43]
Planar 8×8	RMa	5.2	Power; SIR	[44]
Cylindrical	stadium	4.45	PDP of frequency correlation coefficient	[23]
Dipole	similar shopping hall	5.8	Condition number; scalar product	[13]
UCA 64×2	front square	3.33	PDP; PAS	[16]
Virtual 20×20	lecture hall	13-17	Channel gain; K-factor; delay spread; RMS delay spread	[45]
Tx/virtual linear 128×1	hall	2, 4, and 6	PL; PDP	[17]
Tx/ULA 128×8	stadium	1.4725	Channel gains; K-factors; (RMS) composite delay spreads	[7]

AoA: Angle of Arrival
AoD: Angle of Departure
O2I: Ourdoor to Indoor
ODA: Omnidirectional Array
PAS: Power Angular Spectrum
PDP: Power Delay Profile
PL: Path Loss
RMa: Rural Macro
RMS: Root Mean Square
SIR: Signal to Interference Ratio
SNR: Signal Noise Ratio
UCA: Uniform Cylinder Array
ULA: Uniform Linear Array
UMa: Urban Macro
UMi: Urban Micro
UPA: Uniform Planar Array

and 478% more capacity over traditional LTE single-user MIMO with 8Tx-8Rx configuration in macrocells and picocells, respectively. However, the benefit of diversity gains from user equipment (UE) with more antennas falls away as the dimensions of the base station (BS) array increase.

In [9], comparing with the 8 x 8 array, the 16 x 4 array improves the cell-average and cell-edge throughputs by 27% and 71% in Urban Macro (UMa) scenario and enhances the cell-average and cell-edge throughputs by 19% and 43% in Urban Micro (UMi) scenario. When comparing with 8 x 8, the 32 x 2 array enhances the cell-average and cell-edge throughputs by 60% and 112% in UMa and improves the cell-average and cell-edge throughputs by 80% and 118% in UMi scenario. In [10], an effective diversity gain measurement apparatus is proposed to assess diversity performance of multi-antenna systems.

2.2 Eigenvalue Properties and Antenna Array

The measurement in [8] demonstrates that, with the increasing height of user equipment, the BS elevation spreads decrease both in UMa and UMi while the azimuth spreads remain approximately the same. In [11], the condition number is shown to be suitable for measuring both the channel orthogonality between users and the channel harden effect according to the channel measurements in a large lecture hall.

The planar array geometry of a horizontal antenna element is compared with that of a vertical antenna element in [12]. The horizontal antenna arrangement appears to be best suited for massive MIMO operation and yields the lowest average correlation coefficient among the positions considered. According to [13], user proximity and user handgrip reduce the dispersion of the studied properties of the channel across frequencies.

Antenna selection aiming to reduce the number of RF transceiver chains is discussed in [14], in which switching structure and a convex-optimization scheme are presented.

2.3 Non-Stationary Properties

A sufficient interference reduction is obtained in [15] by zero forcing (ZF), whereas maximum ratio combining (MRC) cannot sufficiently reduce the interference when 24 elements are used, even in the 20 GHz band. Moreover, it shows that it is important to select the efficient antennas with high SNR when the antennas cannot be all used. In [6], significant variations in signal strength are characterized for several measured propagation scenarios in the 2.6 GHz frequency range and the change of power variations and correlation properties along with the array is illustrated.

In [16], a measurement campaign performs at the 3.33 GHz in outdoor scenarios, using an antenna array with 64 elements. The results show that the non-stationary properties of the channel over the large array size occur both in delay and spatial domains.

A measurement adopted frequency domain sounder in indoor scenarios in [17] indicates that the channel characteristics of massive MIMO are the non-stationary properties in spatial, delay and frequency domains and the independency between these channel parameters. The carrier frequency is within 2-6 GHz.

Several non-stationary properties of massive MIMO channels in a stadium are investigated in [18], in which the channel parameters appear stationary over the linear antenna array at the high frequency bandwidth (HFB) but not at low frequency bandwidth (LFB). That is because, more stronger Multipath Components (MPCs) appear at LFB due to the smaller path loss and larger obstacle reflection coefficients.

2.4 Multiple Users

In [19], based on the measurements of multiple users (MU) massive MIMO system, spatial separation of closely-spaced users is demonstrated by the analysis and evaluation with the singular value spread.

Channel measurements are performed and corresponding singular value spreads and achieved sum-rate capacities are discussed in [20], and compared with conventional MIMO, massive MIMO is proven to provide better orthogonality between channels for different users and better channel stability.

2.5 Other Channel Characteristics

A flexible testbed is proposed in [21], where the base station operates with up to 100 coherent radio-frequency transceiver chains based on software radio technology.

In [22], an advance MIMO antenna array setup is used to conduct a measurement campaign in Uma propagation. The parameters of all multipath components are extracted with an iterative maximum likelihood high-resolution algorithm (RIMAX). An inter-user interference (IUI) cancellation scheme is also proposed in [22], which simplifies user scheduling method on massive antenna systems for wireless entrance. Besides, the system level simulations using the measured Channel State Information (CSI) confirm that enlarging the angular gap between users reduces spatial correlation and that the IUI cancellation proposal is effective under this condition.

The frequency correlation characteristics using the method of Fourier transform to the channel Power Delay Profile (PDP) are compared with those directly using cross-correlation to the transfer function in a stadium at 4.45 GHz in [23]. It can be determined that the uncorrelated scattering condition and constant means of transfer function are not held.

Angle properties of massive MIMO channels are studied with Multiple SIgnal Classification (MUSIC) and SAGE algorithms based on the channel measurement in outdoor scenarios in [7], in which the Directions of Arrival (DOAs) of the line-of-sight (LoS) signal change with varying geometrical positions in the environment.

The geometric method is used in [24] to characterize the attenuation behavior of the massive MIMO channel with an extended large attenuation matrix proposed. The results in [24] reveal that large attenuation is mostly determined by the transmission distance between the user and the nearest antenna and by the angle with respect to the antenna array as well.

3 Massive MIMO Channel Models

In recent years, many researchers all over the world have advanced the modeling work of massive MIMO channels. The channel models are usually classified into two categories: geometry-based stochastic models (GBSM) and correlation-based stochastic models (CBSM).

GBSMs have been studied extensively to evaluate the performance of wireless channels. These models have the advantage of comprising channel properties accurately. In [25], a novel non-stationary multi-ring channel model on both time and array axes is proposed for massive MIMO systems. With the multi-ring distribution of clusters, the propagation characteristics, such as power imbalance over the array, eigenvalue distribution and antenna correlation, match the conclusions drawn in measurements well. GBSM' direct involvement of scatters/clusters renders it as one of the most promising candidates for 3D MIMO channel modeling [26].

Considering the elevation, the spherical, cylindrical or other kinds of antenna arrays can be adopted. A3D two-cylinder regular-shaped GBSM for non-isotropic scattering massive MIMO channels is proposed in [27], which considers the non-stationary properties, 3D MIMO and spherical wave effect. A 3D wideband twin-cluster channel model is proposed in [28] for massive MIMO communication systems with carrier frequencies on the order of GHz. The near field effect and non-stationary properties are considered. An extension based on the cluster-based COST-2100 MIMO channel model is proposed in [6]. In this model, the channel cannot be seen as wide-sense stationary over the large array at the base station.

CBSMs have lower complexity. They can be categorized into the independent and identically distributed (i.i.d.) Rayleigh fading channel model and correlation channel model. The Kronecker-based stochastic model (KBSM) is one kind of correlation channel models. In [29], a novel KBSM for massive MIMO is proposed, which could capture antenna correlations well. In this model, the evolution of scatters is modeled by the birth-death process and the antenna correlation matrix is equal to the spatial correlation matrix and survival probability matrix. Unlike the i.i.d. Rayleigh channel model, KBSM in [29] considers antenna correlation for the channel model.

4 Analysis of Our Channel Measurement Campaigns

From 2010 to 2014, our team focused on 3D channel measurement and modeling [26] and contributed to 3D channel model standards, 3GPP TR 36.873 [30]. We has started to expand our channel sounder to support the massive MIMO channel measurement and modeling since 2015.

In our measurement work, a 32-element uniform planar array (UPA) was used in the Tx side, and a 16-element dual-polarized omnidirectional array (ODA) was used at the Rx side (**Fig. 1**). The parameters of the antennas are listed in **Table 2** and a straight route was set for the mobile scenario. The measurement campaigns were performed in Urban Macro (UMa), Urban Micro (UMi) and Ourdoor to Indoor (O2I). Here we give an analysis of the UMa measurement. (**Fig. 2**)

To form the massive MIMO array with different antenna

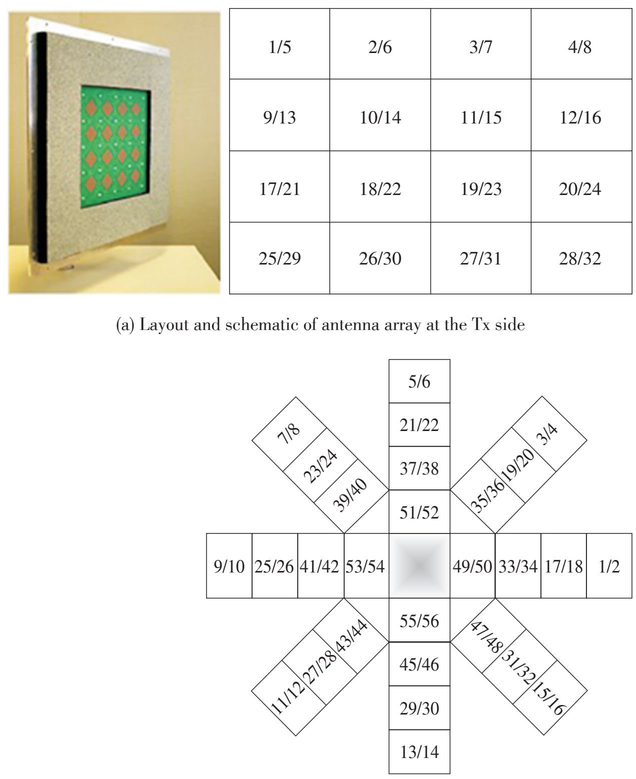

(a) Layout and schematic of antenna array at the Tx side

(b) Layout and schematic of antenna array at the Rx side

▲Figure 1. Antenna layouts used in our measurement work.

▼Table 2. The antenna parameters used in our measurement

Parameter		Value	
Antenna type		ODA (Rx)	UPA (Tx)
Number of antenna ports		56 (#1–#16 were chosen)	32
Overall radiation pattern		Omnidirectional	Hemispherical
Inter element spacing		41.0 mm	41.0 mm
Number of elements		28	16
Angle range	Azimuth	−180° – 180°	−70° – 70°
	Elevation	−70° – 90°	−70° – 70°
Polarized		±45°	±45°
Center frequency		3.5 GHz	
Bandwidth		200 MHz	
PN sequence		255 chips	
ODA: Omnidirectional Array		UPA: Uniform Planar Array	

numbers, our channel measurement campaigns were performed by using the virtual measurement method. **Fig. 3** shows the combining scheme, giving eight adjacent positions. For example, if we wanted to get the data of 64-element virtual antenna array, two groups of CIRs collected from two adjacent positions would be chosen and combined into one group of data. Then we used it as equivalent data collected from 64-element antenna array for further analysis. Similarly, reordering eight groups

▲Figure 2. The overview of the measurement area by Baidu Map (The red triangle is the Tx side; two yellow lines, R1 and R2, represent the measurement route in LoS and non-LoS (NLoS) conditions, respectively; and three red points are in LoS conditions while three blue points are in NLoS conditions).

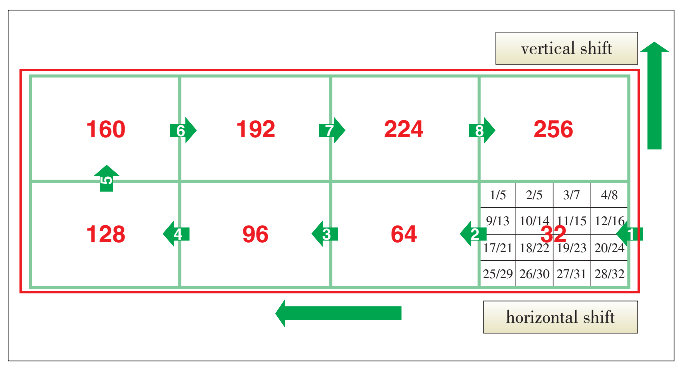

▲Figure 3. The scheme of the antenna combining array in the virtual measurement.

of CIRs to one group could get the data of 256-element virtual antenna array and reordering 4 groups of CIRs to get the data of 128-element virtual antenna array. By the above process, we obtained the data of 256, 128, 64 and 32-element antenna arrays.

To estimate the channel parameters, the SAGE algorithm was used [31], which provides a joint estimation of parameter set $\theta_l=\{\tau_l,f_{d,l},\Phi_l,\Omega_l,\alpha_l\}$, $l=\{1,2,\cdots,L\}$. The τ_l, $f_{d,l}$, Φ_l, Ω_l and α_l denote the propagation delay, the doppler shift, the angle of departure, the angle of arrival and polarization of the l-th propagation sub-path, respectively. Specifically, $\Phi_l=[\theta_{T,l},\phi_{T,l}]$ and $\Omega_l=[\theta_{R,l},\phi_{R,l}]$, where $\theta_{T,l}$, $\phi_{T,l}$, $\theta_{R,l}$ and $\phi_{R,l}$ denote the elevation angle of departure (EoD), angle of departure (AoD), elevation angle of arrival (EoA) and angle of arrival (AoA), respectively. Every 4 snapshots are fed to SAGE to estimate one parameter set.

Finally, to observe the characteristics of clusters, the KpowerMeans clustering algorithm was used to get cluster-level parameters [32], [33]. The multiple path component distance (MCD) is the distance measure for different paths in Kpower-Means. It is a normalized value composing of delay and angular parts.

For delay distance, the definition is given as

$$MCD_{\tau,ij}=\eta\cdot\frac{|\tau_i-\tau_j|}{\Delta\tau}\cdot\frac{\tau_{sd}}{\Delta\tau}. \tag{1}$$

In (1), η is a scaling factor to adjust the weight of delay in the distance function. $\Delta\tau$ means the range of delay and $\Delta\tau=\max_{i,j}|\tau_i-\tau_j|$. τ_{sd} is the standard deviation of delay.

For angle distance, the definition is given as

$$MCD_{T/R,ij}=\frac{1}{2}\left|\begin{matrix}\sin(\theta_i)\cos(\varphi_i) & \sin(\theta_j)\cos(\varphi_j)\\ \sin(\theta_i)\sin(\varphi_i) & -\sin(\theta_j)\sin(\varphi_j)\\ \cos(\theta_i) & \cos(\theta_j)\end{matrix}\right|. \tag{2}$$

For Tx or Rx, the angle distance is obtained in the spherical coordinate system. θ means the elevation angle and φ means the azimuth angle.

The total distance is given by

$$MCD_{ij}=\sqrt{\|MCD_{T,ij}\|^2+\|MCD_{R,ij}\|^2+\|MCD_{\tau,ij}\|^2}. \tag{3}$$

We can see from above equations that MCD consists of angle of arrival, angle of departure, and delay.

4.1 Rationality of the Virtual Measurement

The rationality of the virtual measurement was proved in time and spatial domains [34], the power delay profile (PDP) calculated from combined CIRs and CIRs collected from the measurement campaigns could fit well. Estimated from the combination, the spatial angular characteristics, the elevation angle of departure (EoD), azimuth of departure (AoD), elevation angle of arrival (EoA), and azimuth of arrival (AoA) also matched well with those from the measurement campaigns.

We choose the spot P3 in LoS scenario and the spot P5 in NLoS scenario (Fig. 2) as examples. The other spots in Fig. 2 havesimilar characteristics.

Based on (4), the PDP reconstruction follows the form as (5):

$$\begin{aligned}h_{n,m}(t,\tau_n)=&\begin{bmatrix}F_{rx,n,V}(\Omega_l)\\F_{rx,n,H}(\Omega_l)\end{bmatrix}^T\begin{bmatrix}\alpha_{l,VV} & \alpha_{l,VH}\\ \alpha_{l,HV} & \alpha_{l,HH}\end{bmatrix}\begin{bmatrix}F_{tx,n,V}(\Phi_l)\\F_{tx,n,H}(\Phi_l)\end{bmatrix}\times\\&\exp(jd_n2\pi\lambda_0^{-1}\sin(\Omega_l))\times\\&\exp(jd_m2\pi\lambda_0^{-1}\sin(\Phi_l))\times\exp(j2\pi f_{d,l}t)\end{aligned}, \tag{4}$$

$$P(\tau_n)=\left\|\begin{bmatrix}F_{rx,V}(\Omega_l)\\F_{rx,H}(\Omega_l)\end{bmatrix}^T\begin{bmatrix}\alpha_{l,VV} & \alpha_{l,VH}\\ \alpha_{l,HV} & \alpha_{l,HH}\end{bmatrix}\begin{bmatrix}F_{tx,V}(\Phi_l)\\F_{tx,H}(\Phi_l)\end{bmatrix}\right\|_F^2, \tag{5}$$

where F_{rx} and F_{tx} represent the field patterns of antenna elements in Tx and Rx ends that are generated by the principle of MIMO over-the-air (OTA) test. $\begin{bmatrix}\alpha_{l,VV} & \alpha_{l,VH}\\ \alpha_{l,HV} & \alpha_{l,HH}\end{bmatrix}$ represents the polarized complex amplitude matrix (V stands for vertical polarization and H stands for horizontal polarization).

The SAGE algorithm is a parameter extraction and estimation procedure from the strong path to weak path. One path is characterized by five parameters by SAGE algorithm, and the angular information describes the features of the signal transmission in the space. The rationality of the virtual measurement is discussed by comparing the distribution of paths in the spatial domain with the practical measurement. The power azimuth spectrums (PAS) of practical measured data and virtual measured data in LoS and NLoS scenarios are given, respectively.

Fig. 4a shows the PAS results of angle of departure in the practical measurement in the LoS scenario, while **Fig. 4b** shows the PAS results in the virtual measurement in the LoS scenario. In Fig. 4, the X-coordinate represents the azimuth angle and Y-coordinate represents the elevation angle; the red zone of the label represents the strong path estimated by the SAGE algorithm in the angle of departure and the deep color area represents the weak path which we can mostly ignore because the value of power is lower than −25 dB. The color represents its power in these figures. It is obviously seen that the strong path region is the same in Figs. 4a and 4b and the power values of the strong path are almost equal. Figs. 4c and 4d represent the signal angles in the receiving end; the light color areas there are mostly similar, which means that the major paths are same in the practical and virtual measurements at the same measurement spot. Therefore, in the LoS scenario, the path distribution of the angle domain in virtual measurement is the same as that in practical measurement.

Similarly, **Fig. 5** depicts the PAS results in the NLoS scenario, which are more complex than those in the LoS scenario. According to Fig. 5, the region of the strong path increases in the NLoS scenario. In the transmitting end (Figs. 5a and 5b), the light color areas are more scattered. In the receiving end (Figs. 5c and 5d), it is observed that the number of paths get much more than that in the LoS scenario. With the path number increases, the corresponding departure and arrival angle values of each path in practical and virtual measurements are approximately equal. Therefore, a similar conclusion can be drawn in the NLoS scenario that the path distributions of virtual and practical measurements are almost the same.

4.2 Evolution of Clusters in the Mobile Scenario

The evolution of clusters presents the spatial variation of the massive MIMO channel during the movement [35]. When the mobile station (MS) moves, the power of different clusters varies, and some clusters appear or disappear. Based on the results of clustering, we can get the cluster number evolution

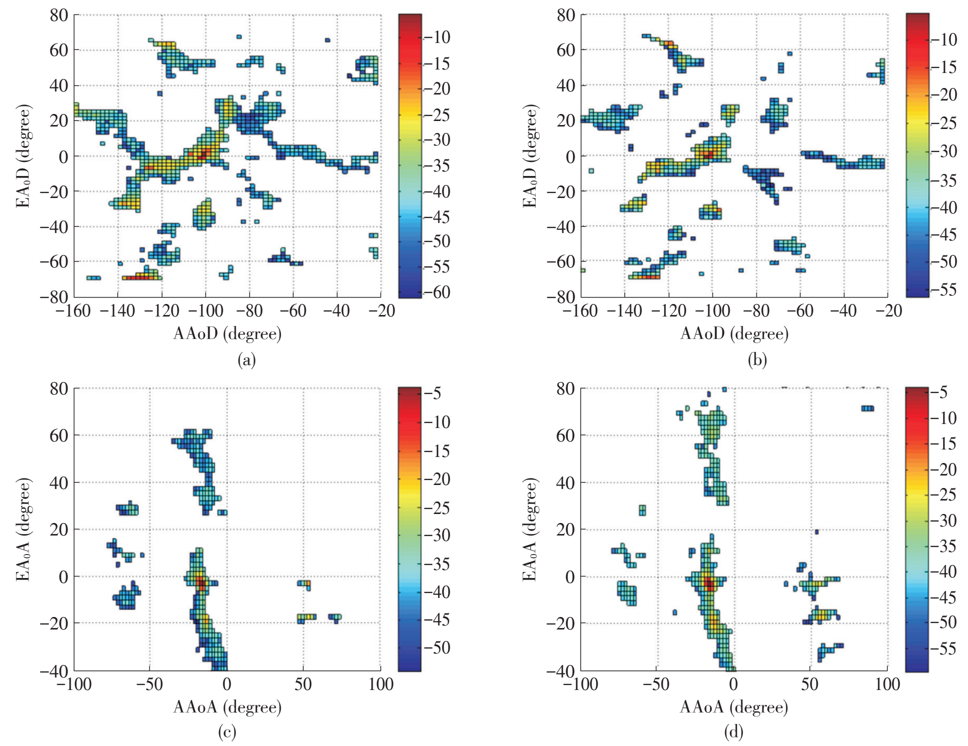

AAoA: Azimuth Angle of Arrival AAoD: Azimuth Angle of Departure EAoA: Elevation Angle of Arrival EAoD: Elevation Angle of Departure

Figure 4.
The PAS results in the LoS scenario: (a) and (c) represent the results from the practical measurement and (b) and (d) represent the results from the virtual measurement.

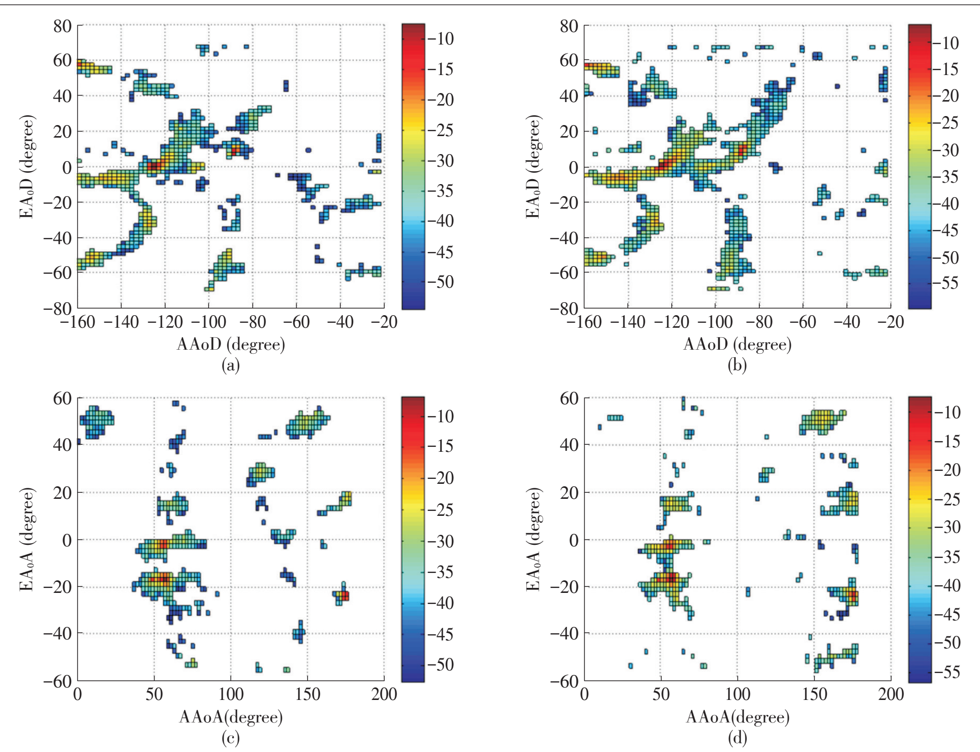

AAoA: Azimuth Angle of Arrival AAoD: Azimuth Angle of Departure EAoA: Elevation Angle of Arrival EAoD: Elevation Angle of Departure

Figure 5.
The PAS results in the NLoS scenario: (a) and (c) represent the results from the practical measurement and (b) and (d) represent the results from the virtual measurement.

(Fig. 6) in R1 (LoS) and R2 (NLoS). The blue curve in Fig. 6 represents LoS conditions, with the average number of clusters is 13.7867; when the distance is 0.5 m, it gets the largest cluster number, 20. On the other hand, the average number is 5.8533 in NLoS conditions (the red curve in Fig. 6), and the largest number is 17 with the distance of 2.9 m and 3 m. There-

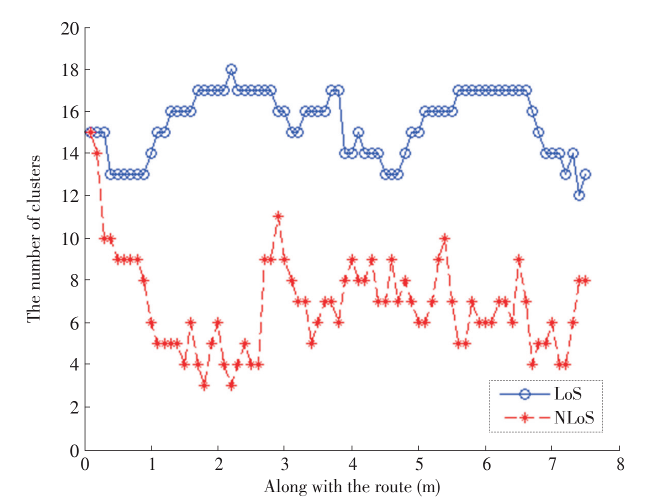

▲Figure 6. The evolution of clusters along with the measurement route.

fore, the cluster number in LoS conditions is more than that in NLoS conditions. This is because the cluster power is normalized and some MPCs' normalized power is too low to keep for clustering. In addition, the cluster number changes more sharply in NLoS conditions than in LoS conditions.

The evolution of clusters was simulated based on the birth-death process that can reflect the non-stationary properties of the clusters. The evolution of clusters $C(i)$, $\{c_1,c_2,\dots,c_R\}$ is expressed as

$$C(i)\xrightarrow{E}C(i+1),(i=1,2,\cdots,R)\,, \tag{6}$$

where R is the evolution number. It depends on the length of measurement route L and observation spacing δ_R along with the route, e.g., when the length of route is 8 m and the observation spacing is set as 0.1 m, the evolution number R is 80.

According to [36], the process of birth and death is assumed to be statistic independent, because the time variation of the channel can also be reflected when MS moves. The main variable in this model is the distance. The birth and death probabilities of each cluster are respectively expressed as

$$\lambda_i=\lambda e^{-\lambda\delta_R D}\,, \tag{7}$$

$$\mu_i=\mu e^{-\lambda\delta_R D}\,, \tag{8}$$

where λ is the cluster newly-generate rate, μ is the cluster disappear rate, δ_R is the observation spacing, and D is the distance correlation factor. Besides, the birth-death process should meet the following conditions

$$\begin{cases} p_{i\,i+1}(t)=\lambda_i(t)+o(t),\ (\lambda_i>0,i=0,1,\cdots,N-1,\lambda_N=0)\\ p_{i\,i-1}(t)=\mu_i(t)+o(t),\ (\mu_i>0,i=0,1,\cdots,N,\mu_0=0)\\ p_{ii}=1-(\lambda_i+\mu_i)t+o(t)\\ p_{ij}(t)=o(t),|i-j|\geqslant 2 \end{cases}. \tag{9}$$

It is noted that the number of clusters is depend on the clustering algorithm. The ratio could be set to tell different clusters and the distance among different MPCs in a cluster. In this case, we wanted show more clusters in NLoS conditions so as to get more information of spatial evolution of clusters.

4.3 Visibility Regions

The concept of visibility region (VR) is proposed by the COST 259, COST 2100 MIMO channel model and more [37], [38]. It is an assumed circular region given in the measurement route. Each VR is related to only one cluster. When the MS moves inside one VR, the corresponding cluster would be active. Otherwise, it would be inactive. With these features, clusters can be observed clearly in mobile scenarios.

Based on the results of clustering, we inferred and calculated the lifetimes of clusters by converting the lifetime to the radius of VR [39], and the cumulative density functions (CDF) of radii of the VRs are presented. To simplify the method, we assume that the MS moves across the center of VRs, i.e., all of the circle centers are distributed along with the route. In LoS conditions, the radii of VRs range from 0.03 m to 2.63 m (**Fig. 7a**), while the radii in NLoS conditions range from 0.03 m to 1.0871 m (**Fig. 7b**), which are less than those in LoS condi-

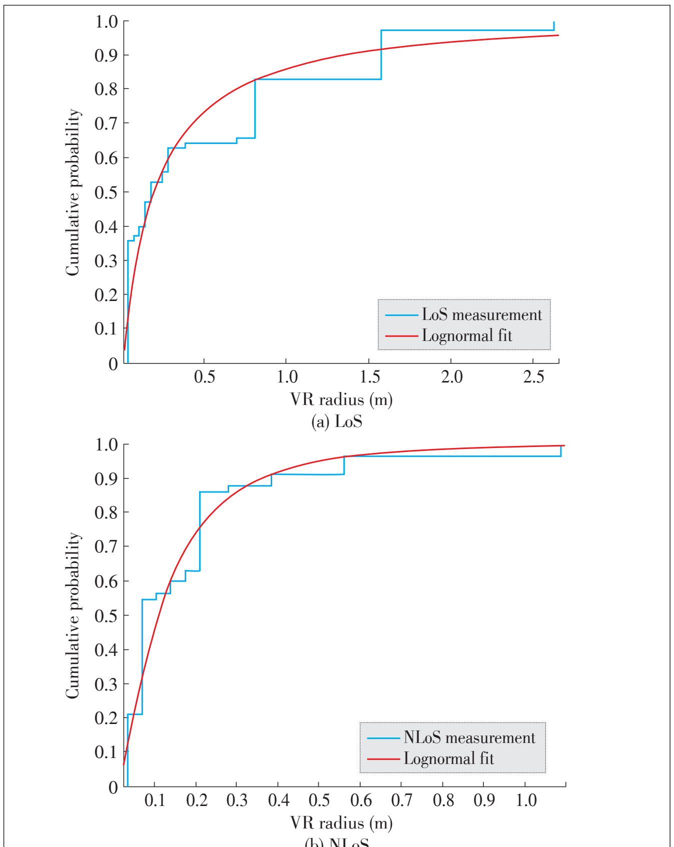

▲Figure 7. The CDFs of radii of VRs in (a) LoS and (b) NLoS conditions.

tions because the appearance and disappearance of clusters occur more frequently. The lognormal distribution fitting is also built, with respect to the measurement curves. The mean and standard deviations of the fitting curves are 0.5180 m and 0.6505 m in LoS conditions and 0.1778 m and 0.2187 m in NLoS conditions, respectively (Fig. 7).

5 Conclusions

In this paper, we summarize the channel measurements and models of massive MIMO system in recent two years. With the increasing number of antennas, the capacity, efficiency and reliability of the system achieve better performance. The channel measurements of channel characteristics including capacity, eigenvalue properties, antenna arrays and MU are analyzed. Based on the channel model categories, the channel models proposed in recent two years are reviewed. The massive MIMO research work by our team is also presented. In our research work, the rationality of massive MIMO virtual measurement is verified and the evolution of clusters of massive MIMO in mobile scenarios is analyzed.

References

[1] N. Czink, X. Yin, H. Özcelik, et al., "Cluster characteristics in a MIMO indoor propagation environment," *IEEE Transactions on Wireless Communications*, vol. 6, no. 4, pp. 1465–1475, Apr. 2007. doi: 10.1109/TWC.2007.05595.

[2] L. Hentilä, M. Alatossava, N. Czink, and P. Kyösti, "Cluster-level parameters at 5.25 GHz indoor-to-outdoor and outdoor-to-indoor MIMO radio channels," in *Proc. 16th IST Mobile and Wireless Communication Summit*, Budapest, Hungary, 2007, pp. 1–5.

[3] J. Poutanen, K. Haneda, J. Salmi, et al., "Analysis of radio wave scattering processes for indoor MIMO channel models," in *IEEE 20th International Symposium on Personal, Indoor and Mobile Radio Communications*, Tokyo, Japan, 2009, pp. 102–106.

[4] T. L. Marzetta, "Noncooperative cellular wireless with unlimited numbers of base station antennas," *IEEE Transactions on Wireless Communications*, vol. 9, no. 11, pp. 3590–3600, Nov. 2010. doi: 10.1109/TWC.2010.092810.091092.

[5] E. Larsson, O. Edfors, F. Tufvesson, and T. Marzetta, "Massive MIMO for next generation wireless systems," *IEEE Communications Magazine*, vol. 52, no. 2, pp. 186–195, Feb. 2014. doi: 10.1109/MCOM.2014.6736761.

[6] X. Gao, F. Tufvesson, and O. Edfors, "Massive MIMO channels—measurements and models," in *Asilomar Conference on Signals, Systems and Computers*, Pacific Grove, USA, 2013, pp. 280–284.

[7] W. Li, L. Liu, C. Tao, et al., "Channel measurements and angle estimation for massive MIMO systems in a stadium," in *17th International Conference on Advanced Communication Technology (ICACT)*, Seoul, South Korea, 2015, pp. 105–108.

[8] Y. Yu, J. Zhang, M. Shafi, et al., "Measurements of 3D channel impulse response for outdoor-to-indoor scenario: capacity predictions for different antenna arrays," in *IEEE 26th Annual International Symposium on Personal, Indoor, and Mobile Radio Communications (PIMRC)*, Hong Kong, China, 2015, pp. 408–413.

[9] G. Liu, X. Hou, F. Wang et al., "Achieving 3D-MIMO with massive antennas from theory to practice with evaluation and field trial results," *IEEE Systems Journal*, vol. PP, no. 99, pp. 1–10, Apr. 2016. doi: 10.1109/JSYST.2015.2477503.

[10] W. J. Liao, B. Y. Dai, and B. R. Hsiao, "Effective diversity gain evaluation for large-scale MIMO antenna system," *IEEE Antennas and Wireless Propagation Letters*, vol. 15, pp. 1394–1397, 2016.

[11] J. Li and Y. Zhao, "Channel characterization and modeling for large-scale antenna systems," in *14th International Symposium on Communications and Information Technologies (ISCIT)*, Incheon, South Korea, 2014, pp. 559–563.

[12] M. Gauger, J. Hoydis, C. Hoek, et al., "Channel measurements with different antenna array geometries for massive MIMO systems," in *10th International ITG Conference on Systems, Communications and Coding*, Hamburg, Germany, 2015, pp. 1–6.

[13] A. O. Martinez, E. De Carvalho, J. O. Nielsen, and L. Jing, "Frequency dependence of measured massive MIMO channel properties," in *IEEE 83rd Vehicular Technology Conference (VTC Spring)*, Nanjing, China, 2016, pp. 1–5.

[14] X. Gao, O. Edfors, F. Tufvesson, and E. G. Larsson, "Multi-switch for antenna selection in massive MIMO," in *IEEE Global Communications Conference (GLOBECOM)*, San Diego, USA, 2015, pp. 1–6.

[15] R. Kataoka, K. Nishimori, N. Tran, and T. Imai, "Basic performance of massive MIMO in indoor scenario at 20-GHz band," in *International Symposium on Antennas and Propagation (ISAP)*, Hobart, Tasmania, 2015, pp. 1–4.

[16] D. Fei, R. He, B. Ai, et al., "Massive MIMO channel measurements and analysis at 3.33 GHz," in *10th International Conference on Communications and Networking in China (ChinaCom)*, Shanghai, China, 2015, pp. 194–198.

[17] J. Li, B. Ai, R. He, et al., "Measurement-based characterizations of indoor massive MIMO channels at 2 GHz, 4 GHz, and 6 GHz frequency bands," in *IEEE 83rd Vehicular Technology Conference (VTC Spring)*, Nanjing, China, 2016, pp. 1–5.

[18] L. Liu, C. Tao, D. W. Matolak, et al., "Stationarity investigation of a LOS massive MIMO channel in stadium scenarios," in *IEEE 82nd Vehicular Technology Conference (VTC Fall)*, Boston, USA, 2015, pp. 1–5.

[19] J. Flordelis, X. Gao, G. Dahman, et al., "Spatial separation of closely-spaced users in measured massive multi-user MIMO channels," in *IEEE International Conference on Communications (ICC)*, London, UK, 2015, pp. 1441–1446.

[20] X. Gao, O. Edfors, F. Rusek, and F. Tufvesson, "Massive MIMO performance evaluation based on measured propagation data," *IEEE Transactions on Wireless Communications*, vol. 14, no. 7, pp. 3899–3911, Jul. 2015.

[21] J. Vieira, S. Malkowsky, K. Nieman, et al., "A flexible 100-antenna testbed for Massive MIMO," in *IEEE Globecom Workshops (GC Wkshps)*, Austin, USA, 2014, pp. 287–293.

[22] S. Sangodoyin, V. Kristem, C. U. Bas, et al., "Cluster-based analysis of 3D MIMO channel measurement in an urban environment," in *IEEE Military Communications Conference (MILCOM 2015)*, Tampa, USA, 2015, pp. 744–749.

[23] Y. Lu, C. Tao, L. Liu, et al., "Frequency correlation investigation of massive MIMO channels in a stadium at 4.45 GHz," in *17th International Conference on Advanced Communication Technology (ICACT)*, Seoul, South Korea, 2015, pp. 271–274.

[24] L. Liu, D. W. Matolak, C. Tao, et al., "Geometry based large scale attenuation over linear massive MIMO systems," in *2016 10th European Conference on Antennas and Propagation (EuCAP)*, Davos, Switzerland, 2016, pp. 1–5.

[25] Q. U. A. Nadeem, A. Kammoun, M. Debbah, and M. S. Alouini, "On the mutual information of 3D massive MIMO systems: an asymptotic approach," in *2015 IEEE International Symposium on Information Theory (ISIT)*, Hong Kong, China, 2015, pp. 2588–2592.

[26] X. Cheng, B. Yu, L. Yang, et al., "Communicating in the real world: 3D MIMO," *IEEE Wireless Communications*, vol. 21, no. 4, pp. 136–144, Aug. 2014. doi: 10.1109/MWC.2014.6882306.

[27] Y. Xie, B. Li, X. Zuo, M. Yang, and Z. Yan, "A 3D geometry-based stochastic model for 5G massive MIMO channels," in *11th International Conference on Heterogeneous Networking for Quality, Reliability, Security and Robustness (QSHINE)*, Taipei, China, Aug. 2015, pp. 216–222.

[28] S. Wu, C. X. Wang, e. H. M. Aggoune, M. M. Alwakeel, and Y. He, "A non-stationary 3-D wideband twin-cluster model for 5G massive MIMO channels," *IEEE Journal on Selected Areas in Communications*, vol. 32, no. 6, pp. 1207–1218, Jun. 2014. doi: 10.1109/JSAC.2014.2328131.

[29] S. Wu, C. X. Wang, E. H. M. Aggoune, and M. M. Alwakeel, "A novel Kronecker-based stochastic model for massive MIMO channels," in *IEEE/CIC International Conference on Communications in China (ICCC)*, Shenzhen, China, 2015, pp. 1–6.

[30] *Technical Specification Group Radio Access Network; Study on 3D channel model for LTE (Release 12. 2. 0)*, 3GPP TR 36.873, 2015.

[31] B. Fleury, M. Tschudin, R. Heddergott, D. Dahlhaus, and K. Ingeman Pedersen, "Channel parameter estimation in mobile radio environments using the SAGE algorithm," *IEEE Journal on Selected Areas in Communications*, vol. 17, no. 3, pp. 434–450, 1999.

[32] D. Du, J. Zhang, C. Pan, and C. Zhang, "Cluster characteristics of wideband 3D MIMO channels in outdoor-to-indoor scenario at 3.5 GHz," in *IEEE 79th Vehicular Technology Conference*, Seoul, South Korea, 2014, pp. 1–6.

[33] C. Huang, J. Zhang, X. Nie, and Y. Zhang, "Cluster characteristics of wideband MIMO channel in indoor hotspot scenario at 2.35GHz," in *IEEE 70th Vehicular Technology Conference Fall (VTC 2009-Fall)*, Anchorage, USA, 2009, pp.

1–5.
[34] H. Yu, J. Zhang, Q. Zheng, et al., "The rationality analysis of massive MIMO virtual measurement at 3.5 GHz," in *IEEE/CIC International Conference on Communications in China (ICCC Workshops)*, Chengdu, China, 2016, pp. 1–5.
[35] C. Wang, J. Zhang, L. Tian, M. Liu, and Y. Wu, "The Spatial evolution of clusters in massive MIMO mobile measurement at 3.5 GHz," presented at VTC2017-Spring, 2017 IEEE 85th Vehicular Technology Conference, Sydney, Australia, 2017.
[36] N. Czink, "The random-cluster model—a stochastic MIMO channel model for broadband wireless communication systems of the 3rd generation and beyond," Dissertation, Telecommunications Research Center Vienna (FTW), 2007.
[37] A. F. Molisch, H. Asplund, R. Heddergott, M. Steinbauer, and T. Zwick, "The COST259 directional channel model—part I: overview and methodology," *IEEE Transactions on Wireless Communications*, vol. 5, no. 12, pp. 3421–3433, Dec. 2006.
[38] R. Verdone and A. Zanella, *Pervasive Mobile and Ambient Wireless Communications: COST Action 2100*. London, UK: Springer-Verlag, 2012.
[39] J. Poutanen, K. Haneda, J. Salmi, V. M. Kolmonen, and P. Vainikainen, "Modeling the evolution of number of clusters in indoor environments," in *Proc. 4th European Conference on Antennas and Propagation*, Barcelona, Spain, Apr. 2010, pp. 1–5.
[40] Y. Zhang, L. Tian, Y. Yu, et al., "3D MIMO channel characteristics and capacity evaluation for different dynamic ranges in outdoor-to-indoor scenario for 6 GHz," presented at IEEE 84th Vehicular Technology Conference VTC2016-Fall, Montreal, Canada, 2016.
[41] Q. Zheng, J. Zhang, H. Yu, Y. Zhang and L. Tian, "Propagation statistic characteristic of 3D MIMO channel in outdoor-to-indoor scenario with different antenna heights", presented at 19th International Symposium on Wireless Personal Multimedia Communications (WPMC 2016), Shenzhen, China, 2015, accepted.
[42] R. Zhang, Z. Zhong, J. Zhao, B. Li, and K. Wang, "Channel measurement and packet-level modeling for V2I spatial multiplexing uplinks using massive MIMO," *IEEE Transactions on Vehicular Technology*, vol. 65, no. 10, pp. 7831–7843, Oct. 2016.
[43] S. Zhang, A. Doufexi, and A. Nix, "Evaluating realistic performance gains of massive multi-user MIMO system in urban city deployments," in *23rd International Conference on Telecommunications (ICT)*, Thessaloniki, Greece, 2016, pp. 1–6.
[44] K. Maruta, A. Ohta, S. Kurosaki, T. Arai, and M. Iizuka, "Experimental investigation of space division multiplexing on massive antenna systems," in *IEEE International Conference on Communications (ICC)*, London, UK, 2015, pp. 2042–2047.
[45] J. Chen, X. Yin, and S. Wang, "Measurement-based massive MIMO channel modeling in 13–17 GHz for indoor hall scenarios," in *2016 IEEE International Conference on Communications (ICC)*, Kuala Lumpur, Malaysia, 2016, pp. 1–5. doi: 10.1109/ACCESS.2017.2652983.

Manuscript received: 2016-11-09

Biographies

ZHANG Jianhua (jhzhang@bupt.edu.cn) received her Ph.D. degree in circuit and system from Beijing University of Posts and Telecommunication (BUPT), China in 2003 and now is a professor of BUPT. She has published more than 100 articles in referred journals and conferences and 40 patents. She was awarded "2008 Best Paper" of *Journal of Communication and Network*. In 2007 and 2013, she received two national novelty awards for her contribution to the research and development of beyond 3G TDD demo system with 100 Mbps@20 MHz and 1 Gbps@100 MHz respectively. In 2009, she received the Second Prize for Science Novelty from Chinese Communication Standards Association for her contributions to ITU-R 4G (ITU-R M.2135) and 3GPP Relay channel model (3GPP 36.814). From 2012 to 2014, she did the 3D channel modeling work and contributed to 3GPP 36.873. She is also the member of the 3GPP 5G channel model for bands up to 100 GHz. Her current research interests include 5G, artificial intelligence, data mining especially in massive MIMO and millimeter wave channel modeling, channel emulator, and OTA test. She is an IEEE senior member and the drafting group (DG) chairwoman of ITU-R IMT-2020 channel model.

WANG Chao (chaowang@bupt.edu.cn) is working for a Ph.D. degree in the Key Lab of Universal Wireless Communications of Ministry of Education, Beijing University of Posts and Telecommunications, China. His current research field is massive MIMO channel measurement and modelling.

WU Zhongyuan (pyboon@foxmail.com) received the B.S. degree from China University of Petroleum, China in 2016. He is currently pursuing a M.S. degree from the Beijing University of Posts and Telecommunication, China. His research interests include massive MIMO channel measurement and modeling, and wireless channel characteristics in 5G system.

ZHANG Weite (zhangweite1994@foxmail.com) is currently a postgraduate student of Beijing University of Posts and Telecommunications (BUPT), China. He received the B.Sc. degree in communication engineering from Shanghai University, China in 2016. His research interests include propagation models, statistical properties of massive MIMO, and machine learning.